IEEE Access
Multidisciplinary | Rapid Review | Open Access Journal

Received 19 February 2023, accepted 10 March 2023, date of publication 14 March 2023, date of current version 20 March 2023.

Digital Object Identifier 10.1109/ACCESS.2023.3257231

RESEARCH ARTICLE

Modified Primary Flux Linkage for Enhancing the Linear Induction Motor Performance Based on Sliding Mode Control and Model Predictive Flux Control

MAHMOUD F. ELMORSHEDY[1,2], (Member, IEEE), DHAFER J. ALMAKHLES[1], (Senior Member, IEEE), AND FAYEZ F. M. EL-SOUSY[3], (Member, IEEE)

[1]Renewable Energy Laboratory, College of Engineering, Prince Sultan University, Riyadh 11586, Saudi Arabia
[2]Electrical Power and Machines Engineering Department, Faculty of Engineering, Tanta University, Tanta 31733, Egypt
[3]Electrical Engineering Department, Prince Sattam bin Abdulaziz University, Al-Kharj 16278, Saudi Arabia

Corresponding author: Mahmoud F. Elmorshedy (mahmoud.elmorshedy@f-eng.tanta.edu.eg)

This study is supported via funding from Prince Sattam bin Abdulaziz University project number (PSAU/2023/R/1444).

ABSTRACT This paper proposes a modified primary flux linkage and an improved weighting less model predictive control for linear induction motors (LIMs) to enhance the drive system in terms of linear speed response, wide speed range, efficiency, and computation time. Sliding mode controller is presented in this work to get quick response instead of the use of the PI controller. A weighting less model predictive flux control (MPFC) is employed to eliminate the weighting factor and reduce the computation time. Furthermore, the optimum value of the primary flux linkage is calculated to guarantee higher efficiency under the operation of maximum thrust per ampere, loss minimization control and wider speed range in the field weakening region. The FCS-MPFC uses only the primary flux in the cost function independent on the weighting factor. Moreover, simplified calculation process can be executed greatly in the $\alpha\beta$-coordinates without transformation matrix, where the end-effect is fully taken into consideration. In comparison with the PI controller under different conditions, the proposed control method can achieve faster dynamics with lower thrust ripple, computation time, and so on. Comprehensive simulation and experimental results based on one prototype with 3 kW linear induction machine have verified the advantages of the proposed strategy in this work.

INDEX TERMS Linear induction machine (LIM), maximum thrust per ampere (MTPA), field weakening, sliding mode control (SMC), finite-control-set model predictive flux control (FCS-MPFC).

NOMENCLATURE

LIM	Linear induction machine.
MTPA	Maximum thrust per ampere.
SMC	Sliding mode control.
FCS	Finite-control-set.
MPFC	Model predictive flux control.
FW	Field weakening.
CCS	Continuous-control-set.
EE	End-effects.
RIM	Rotary induction machine.
VSI	voltage source inverter.
DTC	Direct thrust control.
FOC	Field oriented control.
AIM	Arc induction machine.
LMC	Loss minimization control.

Abbreviations

$u_{\alpha 1}$, $u_{\beta 1}\alpha\beta$	-axes of primary voltage.
$i_{\alpha 1}$, $i_{\beta 1}\alpha\beta$	-axes of primary current.
R_1	Primary resistance.
$\lambda_{\alpha 1}$, $\lambda_{\beta 1}$ $\alpha\beta$	-axes of primary flux linkage.

The associate editor coordinating the review of this manuscript and approving it for publication was Ton Duc Do.

λ_2	Secondary flux linkage.
L_{meq}	Equivalent mutual inductance.
L_{m0}	Mutual inductance at standstill.
F_e	Electromagnetic thrust.
F_l	Load thrust.
τ_l	Pole pitch.
v_2	Linear secondary speed.
M	Mass.
B	Friction.
$f(Q)$	End effect.
λ_{1-opt}	Optimum primary flux linkage.
λ_{2-opt}	Optimum secondary flux linkage.

I. INTRODUCTION

Recently, linear induction machines (LIMs) have been widely applied to linear metro due to their significant advantages of direct linear motion without any transformation gearboxes, which can benefit from strong acceleration or deceleration, great hill-climbing ability, low noise, and so on [1], [2], [3], and [4]. In general, LIMs are derived from the rotary induction machines (RIMs) as the rotor and stator are cut open and then flatted over, as shown in Fig. 1. Till now, there have been more than 30 commercial lines among the world, including the HSST in Tobu-Kyuryo-Line, Guangzhou Subway Line 4 in China, airport rapid transport line in China, Kennedy airline in America, Vancouver light train in Canada, and so on [5], [6], AND [7]. However, the open magnetic circuit of LIM leads the end-effects (EE), brings ill-influence to the drive performance of the whole system, mainly due to that the mutual inductance of LIM varies with the operation speed [8], [9]. In addition, the efficiency of the LIM is lower than the conventional rotary induction machine, where it reaches 80% [10], [11]. Further, nonlinear influence during various working conditions has been generated, which makes its control characteristics more complex than RIM [12].

There are two main control techniques have been used in the traction drive system field-oriented control (FOC) and direct torque control (DTC). FOC method has been widely utilized in the RIM traction drives, yielding excellent performance. The fundamental traction control equation in a region of constant torque holds true for the FOC scheme if the rotor flux (d-axis current) remains constant. In this case, the motor torque will be proportional to the slip frequency (q-axis current). Due to the parameter fluctuations, the traction control rule previously indicated cannot be used in LIM drives. Therefore, several scholars have suggested indirect field-oriented control, direct field-oriented control, and integrated vector and direct thrust control schemes of the LIM in response to Duncan's comparable model. Although these suggested control schemes, the drive performance still low due to slow response, many machine parameters are required, three PI controllers needs to tune, two Clark transformations are needed, and parameter variations.

Meanwhile, DTC has been the method of choice for applications requiring a quick and accurate dynamic thrust response in the small and medium power range. The operation

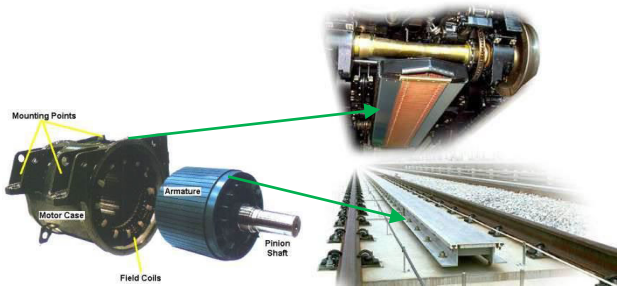

FIGURE 1. Rotary IM in response to LIM.

idea of this control method differs from that of FOC or the vector control methodology. DTC is a method based on primer flux and thrust in the stationary reference frame. The three-level thrust and two-level flux hysteresis comparators are used with the error signals that were collected at the conclusion of the comparison. The best voltage vector is then chosen utilizing the outputs of the comparators and information about where the primer flux is located at the switching table. This choice keeps the thrust error and primer flux inside of their respective hysteresis bands. Yet there are significant drawbacks to this DTC strategy, including the inability to control thrust and flux at very low speeds, high current and thrust ripple, variable switching frequency because hysteresis comparators were used for the thrust and flux comparators, and high noise level at low speeds. Despite the fact that the unique EE may degrade system performance, both field orientation control (FOC) and direct thrust control (DTC) have been mainly employed in the LIM and drive till now [13], [14].

Consequently, model predictive control (MPC) strategies are developed to overcome the problems of the traditional control, and have advantages of online optimization with multivariable control, reduced switching-losses low current distortion, and so on [15], [16], and [17]. In general, the MPC are classified into finite-control-set MPC (FCS-MPC) and continuous-control-set MPC (CCS-MPC) [18], [19]. Furthermore, the FCS MPC has two different types, i.e. the first one is based on predictive current control (FCS-MPCC) and the second is based on predictive thrust control (FCS-MPTC) [3], [20]. Normally, main problems of the FCS-MPCC are the long calculation time resulted from the Clark transformation, and the FCS-MPTC would require weighting factors so as to increase the complexity.

In [21], an experimental comparison between FS-MPCC and FS-MPDTC for conventional RIMs is evaluated. Due to the limited switching state numbers of the three-phase voltage source inverter (VSI) and the discrete nature, the FCS-MPC is used as an alternative solution to the traditional DTC technique when the cost function includes thrust and flux linkage [22]. It is called finite-control-set model predictive thrust control (FCS-MPTC) when the thrust and flux linkages errors are used in the cost function. The operation of the FCS-MPTC is based on selecting the best switching vector, which results in a lower cost function value.

By careful comparison, the FCS-MPC is adopted in this work due to its easy implementation, quick dynamic response, and so on [23]. The traditional cost function of the FCS-MPTC needs a weighting factor to balance the two terms and assigns one term priority over the other [24]. The drive system performance can be improved by reducing thrust ripples and achieving the maximum thrust per ampere (MTPA). This can be ensured by altering and including additional criteria into the cost-function. By adopting this modification, the computation burden and the control complexity will be increased. In addition to these consequences, the system also becomes susceptible to any prediction inaccuracy, which could result in the wrong selection of the switching vectors. Different strategies are developed to achieve the MTPA and reduce the ripples such as presented in [15], [16], and cite17. In [26], the MTPA is presented for conventional rotating machine but it uses four weighing factors in the cost function, which in turn requires tremendous time to obtain the best values [27], [28]. Instead of employing four weighting factors to obtain the MTPA, only one weighting factor for the RIM and the LIM is utilized in [29] and [3], respectively. Further, the weighting less is presented in [30] and [31] where the primary flux linkage term is replaced with similar unit term of thrust or by using cascaded cost functions, respectively. However, the weighting factor is removed but the computational time is increased due to the increase of prediction steps.

Therefore, in order to remove the weighting factor and reduce the calculation steps, this paper removes the thrust error term from the cost function and keeps only the primary flux linkage where this method is called finite-control-set model predictive flux control (FCS-MPFC). In addition, both MTPA, LMC and field weakening criteria are incorporated with this control method to improve the system performance. For further improvement and faster dynamic responses, the outer speed control loop is replaced with the sliding mode control. The influence of the end effect is considered during the machine modelling and the process of the control techniques. This article is organized as follows. Section II discusses the mathematical model of the LIM. In Section III, the FCS-MPC for both thrust control and flux control is presented. Afterwards, the sliding mode control is used to design the speed controller in Section IV. Comprehensive results and discussions are proposed in Section V. Finally, conclusions are drawn in Section VI.

II. MODELLING AND ANALYSIS FOR THE LIM

For the influence of end effect, the LIM dynamic model has some difference compared to those of RIM. In order to make simplification, Duncan dynamic model is used in this work [18], [19]. Therefore, the $\alpha\beta$-axes primary and secondary voltage can be written as

$$u_{\alpha 1} = R_{\alpha 1} i_{\alpha 1} + \frac{\mathrm{d}\lambda_{\alpha 1}}{dt} \tag{1}$$

$$u_{\beta 1} = R_{\beta 1} i_{\beta 1} + \frac{\mathrm{d}\lambda_{\beta 1}}{dt} \tag{2}$$

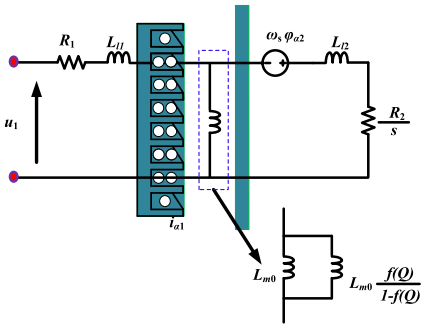

FIGURE 2. Equivalent circuit of the LIM.

$$0 = R_{\alpha 2} i_{\alpha 2} + \frac{\mathrm{d}\lambda_{\alpha 2}}{dt} + (\omega_1 - \omega_2)\,\lambda_{\beta 2} \tag{3}$$

$$0 = R_{\beta 2} i_{\beta 2} + \frac{\mathrm{d}\lambda_{\beta 2}}{dt} + (\omega_1 - \omega_2)\,\lambda_{\alpha 2} \tag{4}$$

$$0 = R_2 \vec{i}_2 + \Delta\vec{\varphi}_2 - j\,(\omega_1 - \omega_2)\,\vec{\varphi}_2 \tag{5}$$

where $\lambda_{\alpha 1}, \lambda_{\beta 1}$ are the $\alpha\beta$-axes primary flux-linkages, $\lambda_{\alpha 2}, \lambda_{\beta 2}$ $\alpha\beta$-axes secondary flux-linkages, while ω_1 and ω_2 the primary and the secondary linear speed, respectively. The primary and secondary flux-linkages based on $\alpha\beta$-axes coordination are given by

$$\lambda_{\alpha 1} = L_1 i_{\alpha 1} + L_{meq} i_{\alpha 2} \tag{6}$$

$$\lambda_{\beta 1} = L_1 i_{\beta 1} + L_{meq} i_{\beta 2} \tag{7}$$

$$\lambda_{\alpha 2} = L_2 i_{\alpha 2} + L_{meq} i_{\alpha 1} \tag{8}$$

$$\lambda_{\beta 2} = L_2 i_{\beta 2} + L_{meq} i_{\beta 1} \tag{9}$$

where L_{meq} is the equivalent mutual inductance considering the end-effect, as calculated from

$$L_{meq} = (1 - f\,(Q))\,L_{m0} \tag{10}$$

where L_{m0} is the mutual inductance at standstill. $f\,(Q)$ represents the dynamic end-effect, as described by [20]

$$f\,(Q) = \frac{\left[1 - \exp\left(-Q\right)\right]}{Q} \tag{11}$$

$$f\,(Q) = \frac{D_s R_2}{(v_2\,[L_{l2} + L_m])} \tag{12}$$

where L_{l2} is the secondary leakage inductance.

The value of the primary and secondary flux-linkages considering the end-effect factor can be calculated from

$$L_1 = L_{l1} + L_{meq} \tag{13}$$

$$L_2 = L_{l2} + L_{meq} \tag{14}$$

Finally, it can get the thrust and motion equations by

$$F_e = \frac{3}{2}\frac{\pi}{\tau}\left(\vec{\lambda}_1^{*} \otimes \vec{i}_1\right) \tag{15}$$

$$F_e = F_l + M\frac{dv_2}{dt} + Bv_2 \tag{16}$$

Fig. 2 illustrates the equivalent circuit of the LIM in the synchronous reference frame.

III. FINITE-CONTROL-SET MODEL PREDICTIVE CONTROL

A. FINITE-CONTROL-SET MODEL PREDICTIVE THRUST CONTROL (FCS-MPTC)

MPC has received increased attention in the last three decades from both academics and industry. The original version of the MPC hypothesis was created at the end of the 1970s. The MPC was utilized in power electronics in 1983. Since 2000, wide-ranging MPC applications in electric drives and power converter systems have been increasingly driven by the significant rise in microprocessor calculation power. Regarding the issues related the traditional control, the finite control set model predictive thrust control strategies is developed. This strategy includes advantages such as online optimization with multivariable control, reduced switching losses, easy to implement, quick dynamic response, low current distortion, and others. Based on these previous advantages, the drive performance can be improved with less effort. For getting faster response, lower thrust ripples, and minimum primary flux-linkage ripples, one FCS-MPDTC is presented for the LIM. The working principles of the FCS-MPTC is like the conventional DTC, where the DTC is based on a previously prepared switching table. But the FCS-MPTC selects the switching vector that gives a minimum value of the cost function. To optimize the efficiency by this control algorithm, it can be elaborated into three essential steps. The first step is parameter estimation, followed by prediction step, and cost function optimization step, which basically plays the main role in choosing the most suitable vector. Main points are summarized as follows.

- *Estimation of primary and secondary flux-linkages can be given by*

$$\vec{\lambda}_1(k) = \vec{\lambda}_1(k-1) + Ts\left(\vec{v}_1(k) - R_1\vec{i}_1(k)\right) \quad (17)$$

$$\vec{\lambda}_2(k) = \frac{L_2}{L_{meq}}\vec{\lambda}_1(k) + \left(L_{meq} - \frac{L_2L_1}{L_{meq}}\right)\vec{i}_1(k) \quad (18)$$

- *Prediction for the primary flux-linkage, $\lambda_1(k+1)$, primary current $i_1(k+1)$, and electromagnetic thrust $F_e(kn+1)$ with the help of first-order Euler method can be given by*

$$\lambda_{\alpha1,i}(k+1) = \lambda_{\alpha1}(k) + T_s\left(u_{\alpha1,i}(k) - R_1 i_{\alpha1}(k)\right) \quad (19)$$

$$\lambda_{\beta1,i}(k+1) = \lambda_{\beta1}(k) + T_s\left(u_{\beta1,i}(k) - R_1 i_{\beta1}(k)\right) \quad (20)$$

$$i_{\alpha1,k}(k+1) = [i_{\alpha1}(k)] \times \left[-\left(\frac{T_s}{Z}\right)\left(R_1 + \frac{R_2}{\tau_l^2}\right) + 1\right] + \left(\frac{T_s}{Z}\right) \times \left(u_{\alpha1,k}(k) + \left(\frac{1}{\tau_r\tau_l} - \frac{\omega_2}{\tau_l}\right)\lambda_{\alpha2}(k)\right) \quad (21)$$

$$i_{\beta1,k}(k+1) = \left[-\left(\frac{T_s}{Z}\right)\left(R_1 + \frac{R_2}{\tau_l^2}\right) + 1\right] \times \left[i_{\beta1}(k)\right] + \left(\frac{T_s}{Z}\right) \times \left(u_{\beta1,k}(k) + \left(\frac{1}{\tau_r\tau_l} - \frac{\omega_2}{\tau_l}\right)\lambda_{\alpha2}(k)\right) \quad (22)$$

$$F_e(k+1) = \frac{3}{2}\frac{\pi}{\tau}\begin{pmatrix}\lambda_{\alpha1}(k+1) * i_{\beta1}(k+1) \\ +\lambda_{\beta1}(k+1) * i_{\alpha1}(k+1)\end{pmatrix} \quad (23)$$

whereas $\tau_r = \frac{L_2}{R_2}$, $Y = \frac{(T_s)}{[L_2+R_2T_s]}$, $Z = \left(L_1 - \frac{L_{meq}^2}{L_2}\right)$, $\tau_l = \frac{L_2}{L_{meq}}$, $u_{\alpha,k}(k)$ and $u_{\beta,k}(k)$ are the $\alpha\beta$-axis voltage vectors. $i_{\alpha1}(k)$ and $i_{\beta1}(k)$ are the $\alpha\beta$-axis measured currents.

$$g_T = \left|F_e^* - F_{e,i}(k+1)\right| + K_1\left|\lambda_1^* - \lambda_{1,i}(k+1)\right| \quad (24)$$

- *Design of the proposed cost function, g_T, is given by*

where K_1 is the weighting factors. One PI controller is used to regulate the linear speed, and then the output of this PI serves as a reference thrust, as used in the cost function.

B. FINITE-CONTROL-SET MODEL PREDICTIVE FLUX CONTROL (FCS-MPFC)

One improved FCS-MPFC is proposed to overcome the use of weighting factor only in the cost function based on the primary flux linkage. The proposed FCS-MPFC reduces the calculation time as only the primary flux is predicted. Similar to the FCS-MPTC, there are three steps for the FCS-MPFC strategy as summarized as follows.

- *Estimation of primary flux-linkage, secondary flux-linkage can be made from (17) and (18). Meanwhile, the thrust is predicted by*

$$F_e = \frac{3}{2}\frac{\pi}{\tau}\frac{1}{\tau_l Z}|\lambda_1||\lambda_2|\sin(\theta_{12}) \quad (25)$$

At fixed value of the primary flux linkage and with assuming constant value for the secondary flux-linkage, the increasing and decreasing rates for the electromagnetic thrust are related to the changing flux angle, θ_{12}. The reference and actual electromagnetic thrusts are given in Fig. 3. The corresponding error of thrust is described by

$$\Delta F_e = F_e^* - F_e = \frac{3}{2}\frac{\pi}{\tau}\frac{1}{\tau_l Z}|\lambda_1||\lambda_2|\left(\sin(\theta_{12} + \delta_{\lambda1}) - \sin(\theta_{12})\right) \quad (26)$$

It is seen from (26) that the error can be regulated by adopting a PI controller, where the output of this PI serves as the increment thrust angle. Based on increment of thrust angle, $\delta\lambda1$ and the estimated angle of the primary flux-linkage, $\theta_{\lambda1}$, with the reference magnitude of the primary flux-linkage, $|\lambda_1^*|$, the reference $\alpha\beta$-axis of the primary flux can be calculated by

$$\lambda_{1\alpha}^* = \left|\lambda_1^*\right|\cos(\theta_{\lambda1} + \delta_{\lambda1}) \quad (27)$$

$$\lambda_{1\beta}^* = \left|\lambda_1^*\right|\sin(\theta_{\lambda1} + \delta_{\lambda1}) \quad (28)$$

- *Prediction for the primary flux-linkage, $\lambda_1(k+1)$, can be made by (19) and (20).*
- *The proposed cost function, g_F, can be given by*

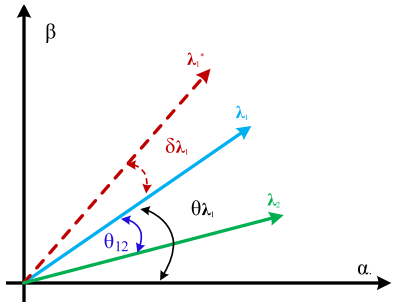

FIGURE 3. Primary and secondary flux-linkage vectors.

$$g_F = \left|\lambda^*_{\alpha 1} - \lambda_{\alpha 1,i}\right| + \left|\lambda^*_{\beta 1} - \lambda_{\beta 1,i}\right| \tag{29}$$

The block diagram of proposed FCS-MPFC for linear speed control in this work is illustrated in Fig. 4.

IV. OPTIMUM CALCULATION FOR PRIMARY FLUX LINKAGE

In this section some detailed discussions about the MTPA and the field weakening region will be presented.

A. MAXIMUM THRUST PER AMPERE

To increase the efficiency of the overall drive system, the value of the flux linkage is set at a certain value, which makes the machine consume a minimum current for the same thrust load, as is known by MTPA. To get the optimum value of the primary flux linkage, the FOC is used in this work, where the whole secondary flux linkage is oriented in the d-axis coordination. After some substituting in the synchronous reference frame dynamic model of the LIM, the relations of the secondary flux linkage and the electromagnetic thrust can be calculated by

$$|\lambda_2| = L_{meq} i_{d1} \tag{30}$$

$$F_e = \frac{3}{2}\frac{\pi}{\tau}\frac{L^2_{meq}}{L_2} i_{d1} i_{q1} \tag{31}$$

For the safe operation, a constraint of the primary current should not exceed their maximum values. Hence, the minimum values of the primary current occur when both d- and q-axes primary currents are equal for the same electromagnetic thrust, which would satisfy the MTPA condition. Aided with this condition and the dynamic model of the LIM in synchronous reference frame, the optimum value of the primary flux-linkage can be obtained from the reference thrust to achieve the MTPA condition, as given by

$$\lambda^*_{1MTPA} = \sqrt{L_1^2 + (L_1 - \frac{L^2_{meq}}{L_2})^2} * \sqrt{F^*_e / \left((3\pi L^2_{meq})/(2\tau L_2)\right)} \tag{32}$$

B. FIELD WEAKENING REGION

Normally, the primary voltage of LIM should overcome the voltage drop of primary resistance and the back electromotive force (BEMF). At fixed primary flux-linkage, the BEMF is proportional to the linear speed. Meanwhile, the linear speed goes up to the rated value, the primary voltage has to increase over the rated. But due to the limitations in the applied voltage, the primary flux-linkage level can be decreased (named by the field weakening). Hence, in order to get the optimum value for the primary flux linkage at higher linear speed, the following analysis would be firstly presented based on the FOC. At stead-state condition, the dq-axis voltage relations are described by

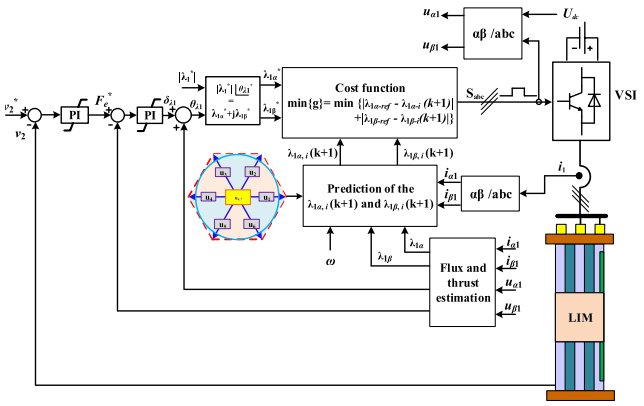

FIGURE 4. The proposed FCS-MPFC for the LIM.

$$v_{d1} = -\omega_1 Z i_{q1} \tag{33}$$

$$v_{q1} = \omega_1 L_1 i_{d1} \tag{34}$$

The voltage limitation can be calculated in terms of dq-axis primary currents, as illustrated by

$$\frac{v^2_{max}}{\omega_1^2} \geq L_1 i^2_{d1} + Z i^2_{q1} \tag{35}$$

The limitations loci for both voltage and current are shown in Fig. 5, respectively. It is noticed that the current constraint is a circle. Meanwhile, the voltage constraint is ellipse shrink at higher speed. The electromagnetic thrust subject to the current is indicated by the dot red line. Above the rated speed, both voltage and current limit determine the operating point. Hence, the values of the dq-axis currents are given by

$$i^*_{d1} = \sqrt{\frac{\left(\frac{v_{\max}}{\omega_1}\right)^2 - (ZI_{\max})^2}{L_1^2 - Z^2}} \tag{36}$$

$$i^*_{q1} = \sqrt{I^2_{\max} - i^{2*}_{d1}} \tag{37}$$

From (30) and (31), the value of the primary flux linkage and the electromagnetic thrust can be obtained from

$$\lambda^*_{1FW} = L_{meq} \sqrt{\frac{\left(\frac{v_{\max}}{\omega_1}\right)^2 - (ZI_{\max})^2}{L_1^2 - Z^2}} \tag{38}$$

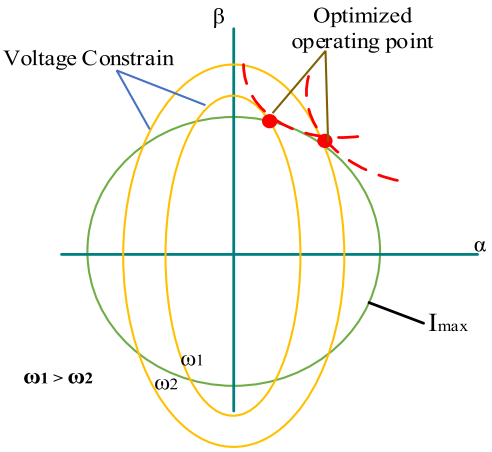

FIGURE 5. Primary current and voltage limitations.

$$F_e^* = \frac{3}{2}\frac{\pi}{\tau}\frac{L_{meq}^2}{L_2}\sqrt{\left(\frac{\left(\frac{v_{\max}}{\omega_1}\right)^2 - (ZI_{\max})^2}{L_1^2 - Z^2}\right)\left(I_{\max}^2 - i_{d1}^{2*}\right)} \tag{39}$$

C. LOSS MINIMIZATION CONTROL

To reduce the losses based on the FCS-MPFC, the optimal primary flux linkage is calculated. The following steps are used to find the optimum flux linkage for achieving the loss minimization. Firstly, the power loss can be calculated from the following equation.

$$P_{loss} = R_1\left(i_{d1}^2 + i_{q1}^2\right) + R_2\left(i_{d2}^2 + i_{q2}^2\right) \tag{40}$$

Based on the FOC, the dq-axis currents for both primary and secondary can be calculated from the following relations

$$i_{d1} = \frac{\lambda_2}{L_{meq}} \tag{41}$$

$$i_{q1} = \frac{2}{3}\frac{\tau}{\pi}\frac{L_2}{L_{meq}}F_e\lambda_2^{-1} \tag{42}$$

$$i_{d2} = 0 \tag{43}$$

$$i_{q2} = -\frac{2}{3}\frac{\tau}{\pi}F_e\lambda_2^{-1} \tag{44}$$

The power loss in terms of the secondary flux linkage can be obtained as follows:

$$P_{loss} = R_1\left(i_{d1}^2 + i_{q1}^2\right) + R_2\left(i_{d2}^2 + i_{q2}^2\right) \tag{45}$$

$$P_{loss} = R_1\left(\frac{\lambda_2}{L_{meq}}\right)^2 + R_1\left(\frac{2}{3}\frac{\tau}{\pi}\frac{L_2}{L_{meq}}F_e\lambda_2^{-1}\right)^2 R_2\left(-\frac{2}{3}\frac{\tau}{\pi}F_e\lambda_2^{-1}\right)^2 \tag{46}$$

$$P_{loss} = R_1\left(\frac{\lambda_2}{L_{meq}}\right)^2 + R_1\left(\frac{L_2}{L_{meq}}\right)^2\left(\frac{2}{3}\frac{\tau}{\pi}F_e\lambda_2^{-1}\right)^2 + R_2\left(-\frac{2}{3}\frac{\tau}{\pi}F_e\lambda_2^{-1}\right)^2 \tag{47}$$

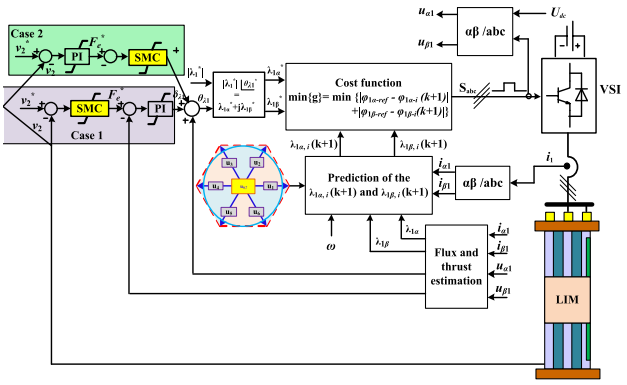

FIGURE 6. The proposed FS-MPFC with SMC for the outer speed loop.

$$P_{loss} = R_1\left(\frac{\lambda_2}{L_{meq}}\right)^2 + \left[R_1\left(\frac{L_2}{L_{meq}}\right)^2 + R_2\right]\left(\frac{2}{3}\frac{\tau}{\pi}F_e\lambda_2^{-1}\right)^2 \tag{48}$$

$$P_{loss} = \frac{1}{L_{meq}^2}\left[R_1\lambda_2^2 + \left(R_1L_2^2 + R_2L_{meq}^2\right)\left(\frac{2}{3}\frac{\tau}{\pi}F_e\lambda_2^{-1}\right)^2\right] \tag{49}$$

Assuming that none of the motor parameters affects the secondary flux, $\lambda_{2-\text{opt}}$ can be obtained, under a constant thrust load, by setting the derivative of equation (45) to zero.

$$\frac{\partial P_{loss}}{\partial \lambda_2} = 0 \tag{50}$$

The optimum value of the secondary flux linkage which the loss minimization can be achieved is given by

$$\lambda_{2-opt} = \sqrt{\left(\frac{2}{3}\frac{\tau}{\pi}L_{meq}\right)F_e\sqrt{\frac{\left(R_1L_2^2 + R_2L_{meq}^2\right)}{R_1}}} \tag{51}$$

After some substitution, the optimal value of the primary flux linkage, which the loss minimization can be achieved, is obtained from

$$\lambda_{1-opt} = \frac{L_1}{L_{meq}}\sqrt{\lambda_{2-opt}^2 + \left(\sigma\frac{2}{3}\frac{\tau}{\pi}\right)^2\left(\frac{F_e}{\lambda_{2-opt}}\right)^2} \tag{52}$$

V. SLIDING MODE CONTROL FOR LINEAR SPEED AND THRUST

Sliding mode control (SMC) has been widely applied to RIMs owing to the fast dynamic responses [21], [22], [23]. But for LIMs, there are a few literatures of SMC with the traditional control [24], [25]. In this article, the FCS-MPFC is improved by using the SMC for the outer linear speed control loop in the first case as illustrated in Fig. 6. Meanwhile, the second case is used for the inner control loop to regulate the electromagnetic thrust instead of the PI control loop as shown in Fig. 6. An external load disturbance is added to the modified motion equation, as given by

$$v_r^{\bullet} = -(\frac{1}{M} + \Delta\frac{1}{M})F_e + (\frac{1}{M} + \Delta\frac{1}{M})F_l + (\frac{1}{M} + \Delta\frac{1}{M})Bv_r \tag{53}$$

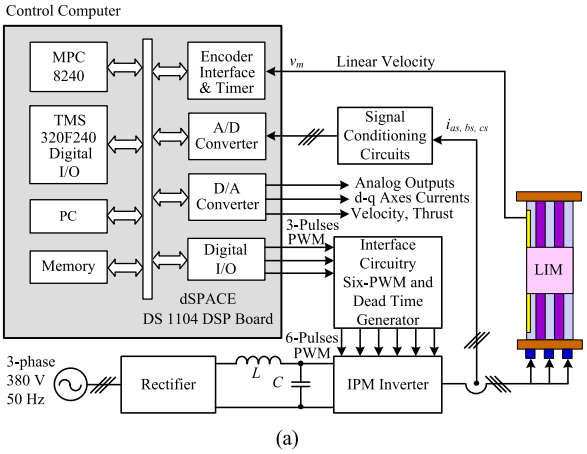

(b)

FIGURE 7. Testing bench of the LIM.

TABLE 1. Main Parameters of the AIM.

Parameter	Symbol	Value
Nominal power	P_n	3 kW
Nominal linear velocity (mechanical)	v_m	11 m/sec
Rated thrust	F_e	300 N
Rated current	I	20 A
Primary windings resistance	R_1	1 Ω
Secondary windings resistance	R_2	2.4 Ω
Mass of the mover	M	143 kg
Secondary leakage inductance	L_{l2}	0.0043H
Pole pitch	τ_p	

$$v_r^{\bullet} = -\frac{1}{M}F_e + \Delta X + \frac{1}{M}v_r \tag{54}$$

where B is the viscous coefficient, M the total mass of LIM, and ΔX the lumped uncertainty that can be expressed by

$$\Delta X = \Delta\frac{1}{M}F_e + (\frac{1}{M} + \Delta\frac{1}{M})F_l + \Delta\frac{1}{M}v_r \tag{55}$$

After that, a control law is required to get a perfect tracking to the reference v_r^*. One sliding mode surface, s, is used in this work, as defined by a function of speed tracking error ε_v. The error state for the speed is designed by

$$\left.\begin{aligned} \varepsilon_v &= v_r^* - v_r \\ x_v &= \varepsilon_v^{\bullet} = v_r^{\bullet *} - v_r^{\bullet} \end{aligned}\right\} \tag{56}$$

$$v_r^{\bullet} = \frac{1}{M}F_e + \Delta X + \frac{1}{M}v_r \tag{57}$$

From the previous equations, the variable SM surface is given by

$$s = k^*\varepsilon_v + x_v \tag{58}$$

where k is a positive constant of the SMC variable. To diminish the negative effects on the SMC, one improved reaching law is proposed to reduce the chattering phenomena and meanwhile guarantee fast response, as given by

$$s^{\cdot} = -\varepsilon sgn(s) - Ds \tag{59}$$

where the switching gain ε and the exponent coefficients of reaching law, D, are greater than zero. At $s = s^{\bullet}$, the states of drive system reach the sliding surface, as expressed by

$$-\varepsilon sgn(s) - Ds = k^*\varepsilon_v^{\bullet} + x_v^{\bullet} \tag{60}$$

Finally, the reference thrust is calculated by

$$F_e^* = \frac{\left(k^* v_r^{\bullet *} + v_r^{*\bullet\bullet} + \varepsilon sgn(s) + Ds\right)}{\frac{-1}{M}} + \frac{\left(D * F_l\hat{} - \frac{D}{M}v_r - \frac{1}{M}v_r^{\bullet}\right)}{\frac{-1}{M}} \tag{61}$$

where k, ε, and D are variable state coefficients for the SMC, which can reach zero in one finite time. The function ***sgn(s)*** is replaced by $sat(s) = \frac{s}{s+\gamma}$ to reduce the external disturbance and undesirable chattering effect [24]. γ is a small positive constant. On the other hand, for the second case (i.e., the inner control loop of thrust), the output of the SMC serves as the increment of the primary flux linkage angle. It is seen that this increment is very small due to the chattering of the SMC. Hence, the first case is presented in this article.

VI. SIMULATION AND EXPERIMENTAL RESULTS

This part validates the MTPA, LMC and the FW based on sliding mode control and model predictive flux control under different operating conditions by comprehensive simulation and experimental results. The prototype is given in Fig. 7, which consists of 3kW linear induction machines (LIM) which are used to check the drive performance under acceleration, deceleration, loading change, speed change, high-speed cruising, breaking, etc. In brief, the drive system is composed of a rectifier and voltage source inverter, a dSPACE 1104 based control board, and so on.

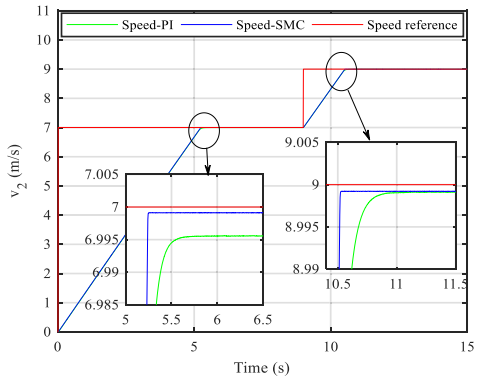

FIGURE 8. SMC and PI control for speed response during change in the reference speed.

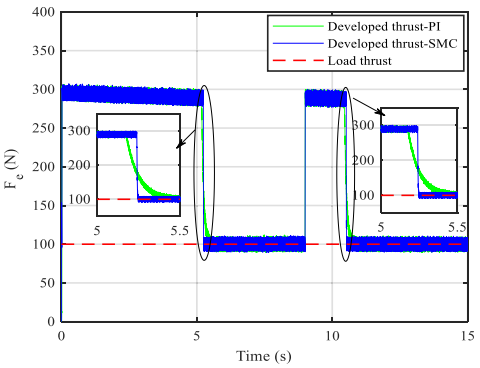

FIGURE 9. Electromagnetic thrust responses under speed variation for both SMC and PI control.

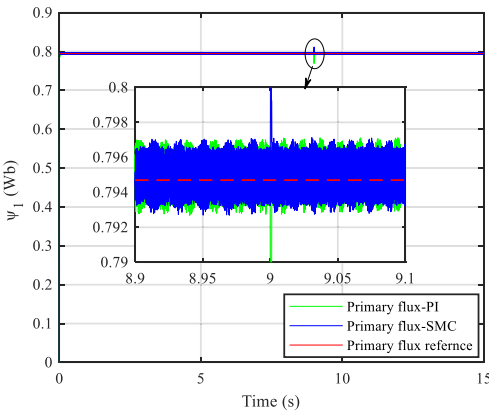

FIGURE 10. Primary flux-linkage under speed variation for both SMC and PI control.

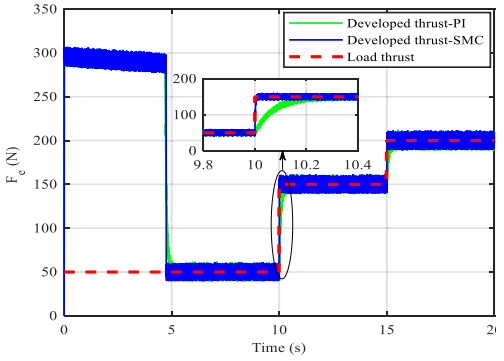

FIGURE 11. Electromagnetic thrust and load profile for SMC and PI control with FCS-MPFC at constant reference speed.

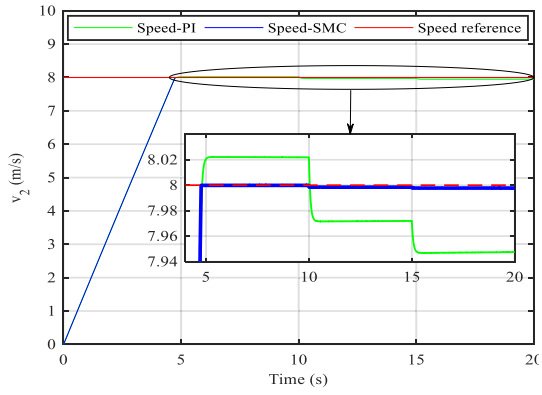

FIGURE 12. Speed response under load variation for SMC and PI control with FCS-MPFC.

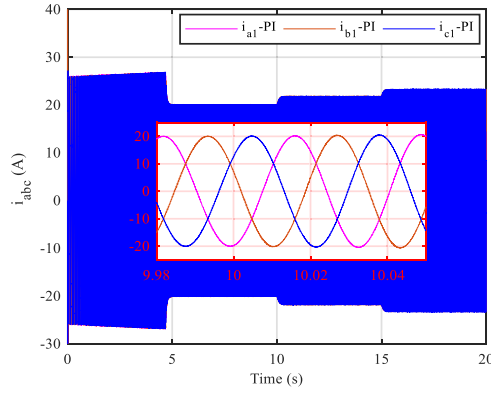

FIGURE 13. Primary current response with outer control loop of PI and with FCS-MPFC for load variation.

A. SIMULATION RESULTS AND ANALYSIS

Comprehensive simulation studies are proposed under different operating conditions based on both SMC and PI, including speed variation, thrust variation, and speed variation with and without MTPA and LMC. During the different cases the range of the linear speed changes with different levels starting from 7 m/s up to 13 m/s to check the proposed SM control with different techniques of MTPA and FW. The rated speed of the LIM is 11 m/s. Main parameters of the used arc induction machine (AIM) are given in Table 1.

- *Case 1. Speed variation without MTPA*

In this case, detailed comparison analysis between the SMC and the PI control for the outer linear speed loop is made, where the reference speed is changed from 7 m/s to 9 m/s, where the load is fixed at 100 N. The FCS-MPFC is used in the inner control loop, which can generate the best switching vector to the inverter. Figure 8 illustrates the reference, actual

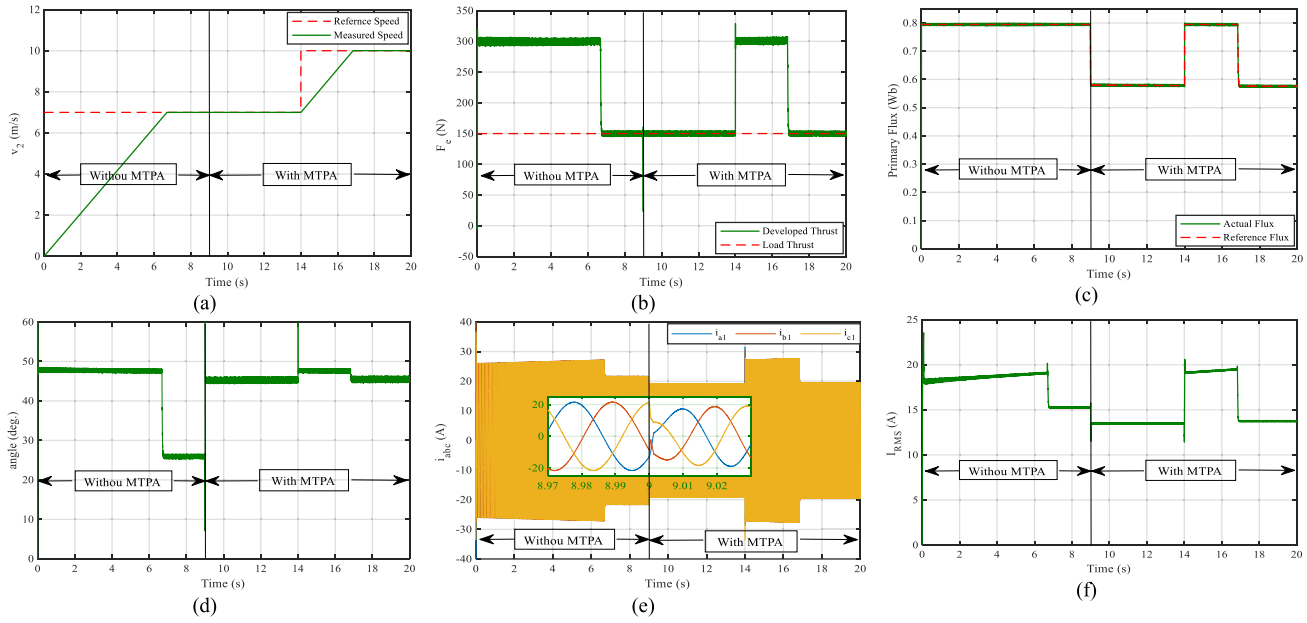

FIGURE 14. Performance of the PI outer control loop with and without MTPA based FCS-MPFC under speed variation. (a) Speed. (b) Thrust. (c) Primary flux(d) Angle. (e) Three phase currents. (f) RMS current.

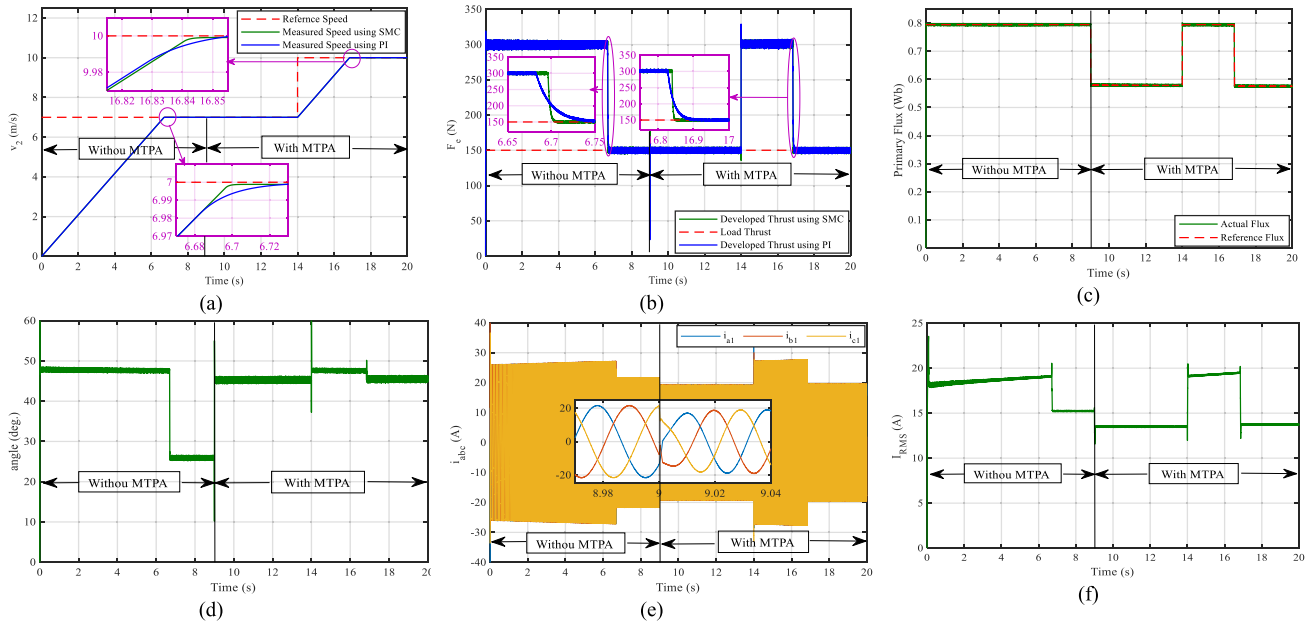

FIGURE 15. Performance of the SMC outer control loop with and without MTPA based FCS-MPFC under speed variation. (a) Speed. (b) Thrust. (c) Primary flux(d) Angle. (e) Three phase currents. (f) RMS current.

PI speed, and actual SMC speed. It is noted that the SMC can get much quicker dynamic speed and smaller steady-state error than the PI control. Figure 9 shows the response of the electromagnetic thrust with the load thrust for both SMC and the PI controllers. The electromagnetic thrust based on the SMC can track the load thrust much faster compared to the PI controller. As to the primary flux linkage, as shown in Fig.10, the two control methods can get similar ripples with each other. For a quantitative comparison, Table 2 gives the speed rising time and the steady state error for both PI and SMC.

- *Case 2. Load variation without MTPA*

The performance of the drive system is tested under three levels of load (50 N, 150 N, and 200 N) with constant reference speed 8 m/s. Both SMC and PI control responses for the electromagnetic thrust are illustrated in Fig. 11. It is observed that the SMC has faster response in comparison to the PI controller. Figure 12 shows the effect of the load

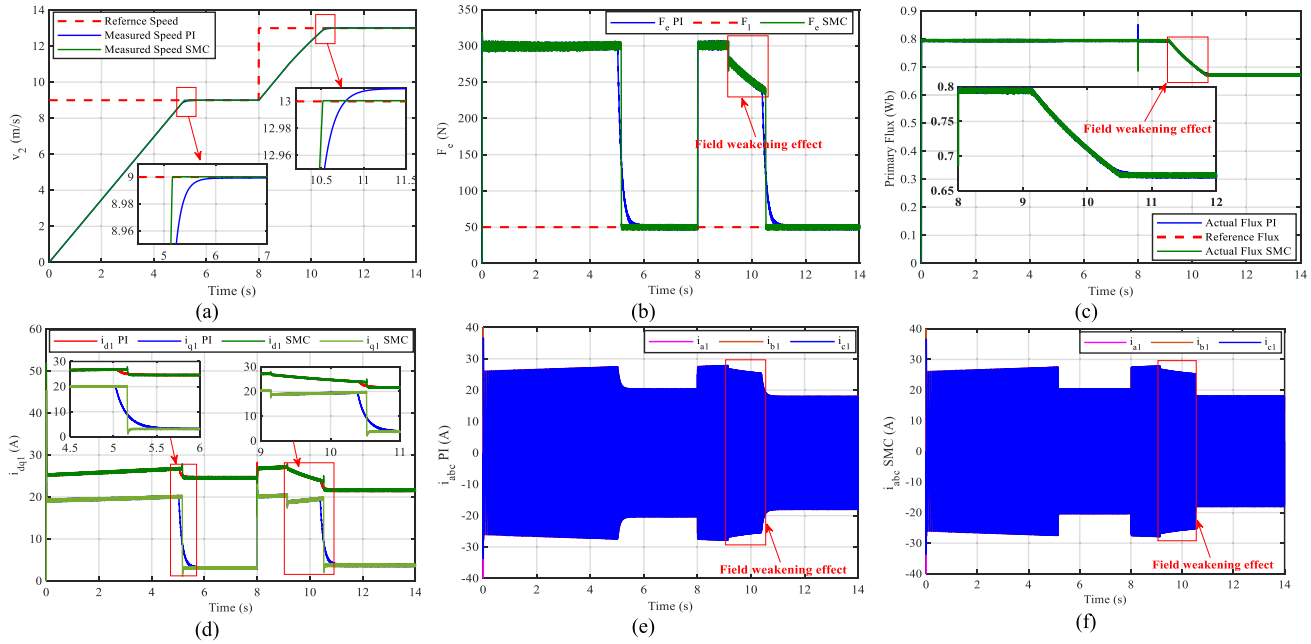

FIGURE 16. Performance of the PI and SMC outer control loop under overrated speed based FCS-MPFC. (a) Speed. (b) Thrust. (c) Primary flux(d) dq-axis currents. (e) Three phase currents using SMC. (f) Three phase currents using SMC.

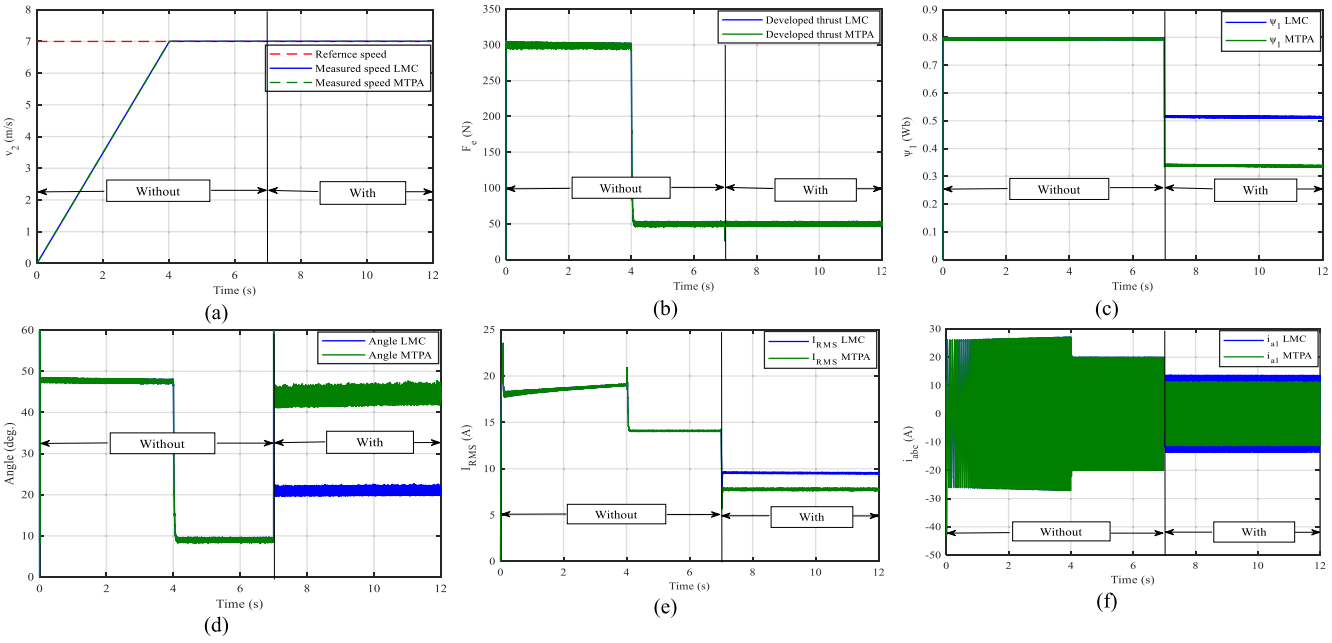

FIGURE 17. Comparison between the responses of the FCS-MPFC based on the MTPA and the LMC. (a) Speed. (b) Developed thrust. (c) Primary flux linkage. (d) Angle difference. (e) RMS primary current. (f) three phase primary currents.

variation on the actual speed, where the SMC can keep good tracking with the reference value, while the PI would suffer a little error as the loading changes. The three-phase primary currents are similar for PI control and SMC as illustrated in Fig. 13. Further, the quantitative comparison results are listed in Table 3.

- *Case 3. Speed variation with MTPA*

In this case, the proposed drive system based on SMC and PI with FCS-MPFC is tested under different speed variation with and without MTPA in the same working condition. The reference linear speed changes from 7 m/s to 10 m/s as illustrated in Figs. 14 (a) and 15 (a) for both PI and SMC, respectively. Meanwhile, the load is fixed constant at 150 N as shown in Figs. 14 (b) and 15 (b). Both control methods are succeeded in regulating the actual speed, where the SMC can get a much quicker response. After 9 s, the optimum flux is used to achieve the MTPA as given in Figs. 14 (c) and 15 (c). Once the optimum flux is applied, the angle difference can get the

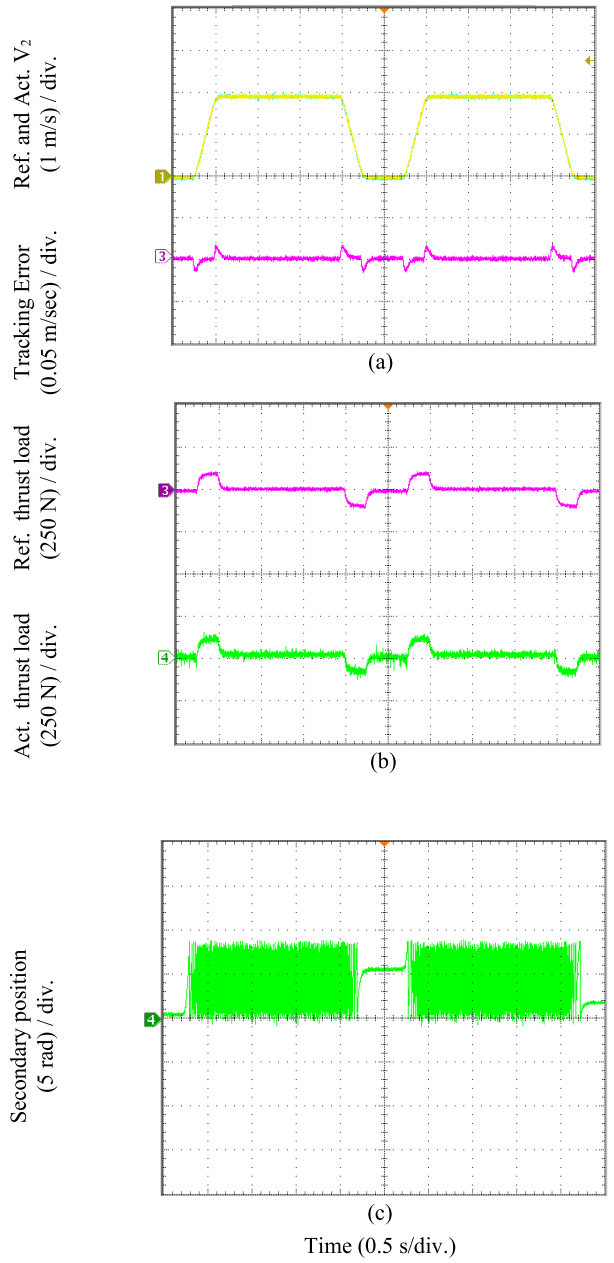

FIGURE 18. Performance of the PI outer control loop based on FCS-MPFC under speed variation and no load. (a) Reference speed, actual speed, speed tracking error. (b) Reference and actual thrust. (c) Secondary position.

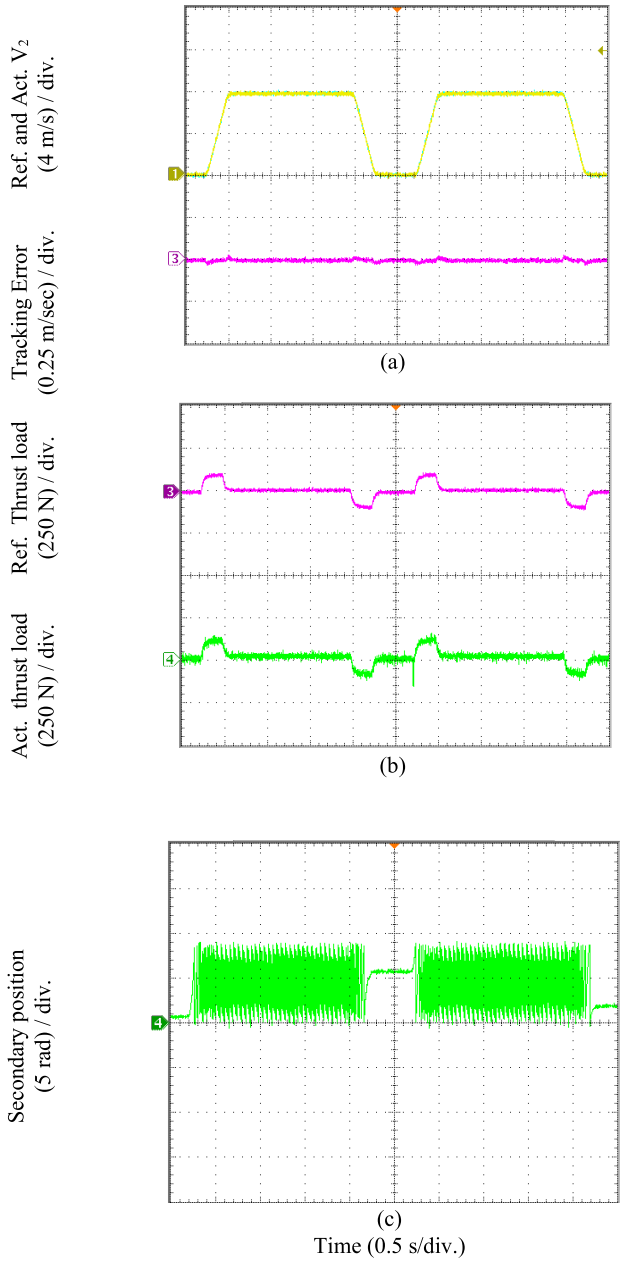

FIGURE 19. Performance of the SMC outer control loop based on FCS-MPFC under speed variation and no load. (a) Reference speed, actual speed, speed tracking error. (b) Reference and actual thrust. (c) Secondary position.

TABLE 2. Quantities Responses Between SMC and PI During Speed Variations.

Quantity	SMC	PI
Speed rising time (s)	5.2	5.7
Steady state speed error (m/s)	0.0001	0.005

TABLE 3. Quantities responses Between SMC and PI During Load Variations.

Quantity	SMC	PI
Steady state speed error (m/s)	0.0005	0.02
Speed rising time (s)	4.9	5.3

best value of 45o, and thereof the three phase instantaneous currents would decrease, as shown in Figs.14 (d) and (e), and Figs. 15 (d) and (e), respectively. It is noted that the RMS primary current can be reduced by 2 A.

- *Case 4. Performance of the drive system above rated speed*

In this case, the speed of the drive system is increased over the rated speed to check the drive system in the field weakening region, where both SMC and PI are used in the outer speed

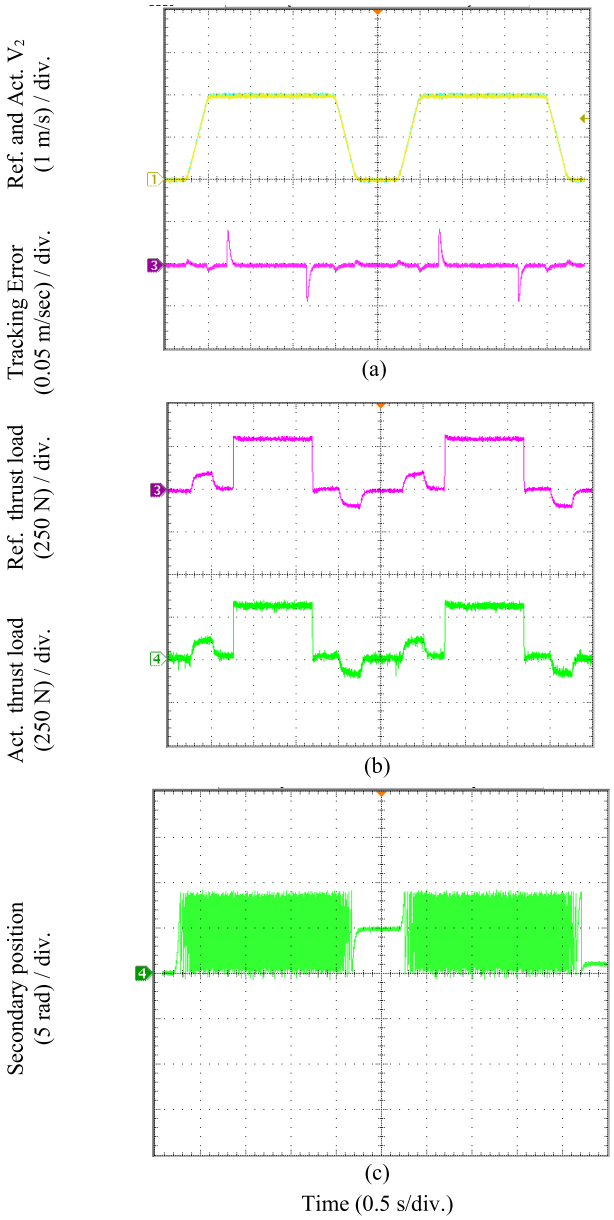

FIGURE 20. Performance of the PI outer control loop based on FCS-MPFC under speed variation and no load. (a) Reference speed, actual speed, speed tracking error. (b) Reference and actual thrust. (c) Secondary position.

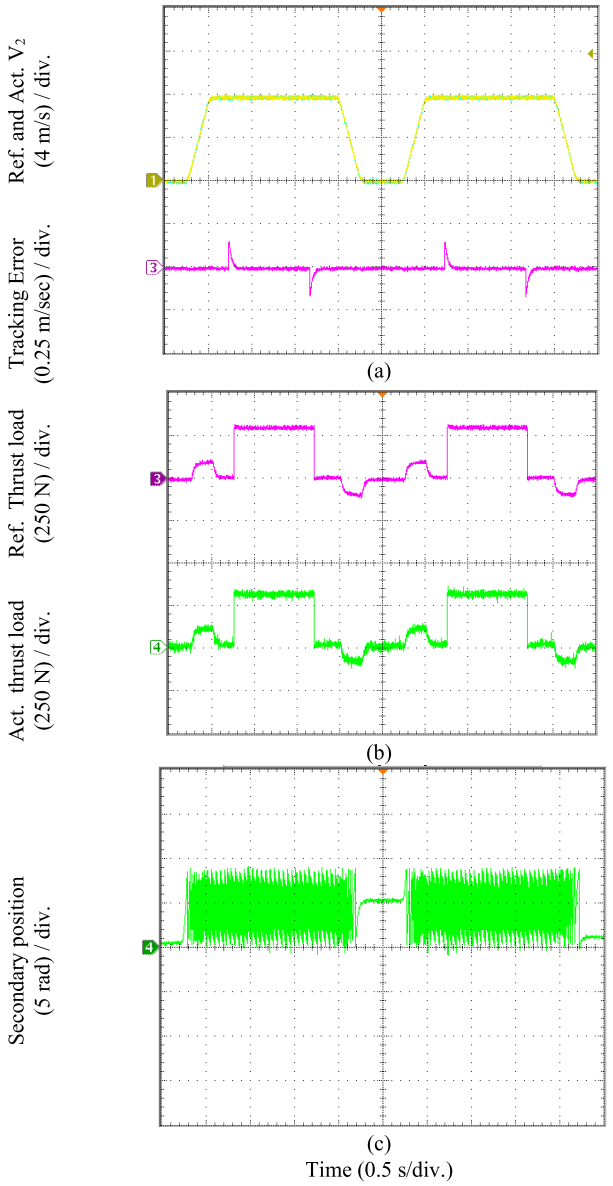

FIGURE 21. Performance of the SMC outer control loop based on FCS-MPFC under speed variation and no load. (a) Reference speed, actual speed, speed tracking error. (b) Reference and actual thrust. (c) Secondary position.

loop. The reference linear speed is increased from 9 m/s up to 13 m/s as illustrated in Fig. 16 (a). It can be observed that the control works well, and the speed tracks the reference value, but the SMC achieves faster response. The thrust load is 50 N as indicated in Fig. 16 (b). It is noticed that when the speed reaches over the rated speed, the maximum thrust value is decreased to keep the safety operation. Hence, the rate of increasing speed is decreased, which takes time to reach the reference value. The values of the primary flux linkage and the dq-axis currents during PI and SMC are given in Figs. 16 (c) and (d). It is observed that the values of the primary flux linkage and the d-axis current are decreased when the speed goes up over the rated speed. The three-phase instantaneous currents responses are shown in Figs. 16 (e) and (f) for PI and SMC respectively.

- *Case 5. Compared performance of the drive system based on LMC and MTPA*

To illustrate the difference between the MTPA and the LMC, this case study has been presented. In this studying case the same speed of 7 m/s and the same thrust of 5 N has been applied. The two-control method has been activated after 7 seconds. Figure 17 shows the comparison responses for both the MTPA and the LMC. It can be noticed that the two control methods succeeded in regulating the actual speed at the reference value and achieving the thrust load as shown

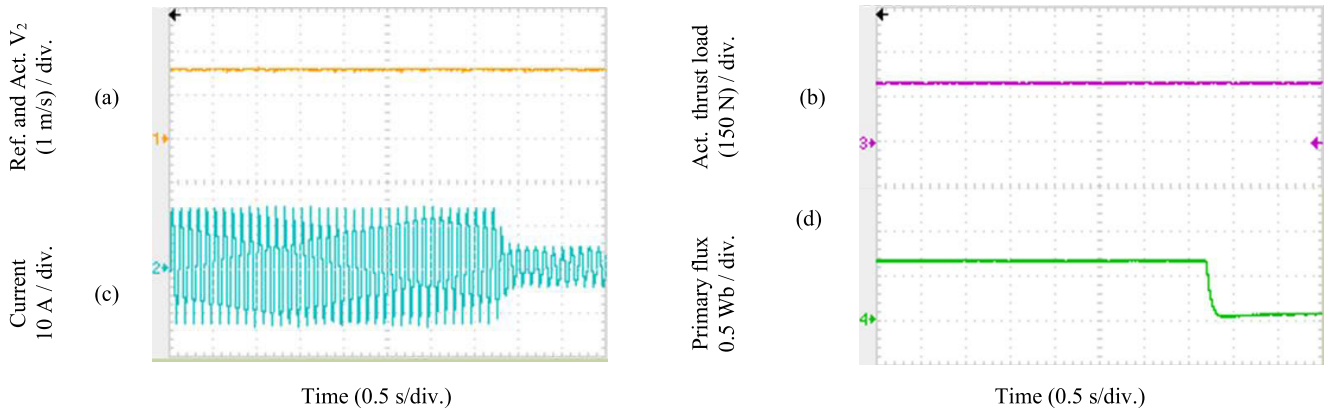

FIGURE 22. Response of LIM drive system using the proposed FCS-MPFC with MTPA. (a) Reference speed, (b) Actual thrust. (c) Primary current. (d) Primary flux linkage.

TABLE 4. Main Parameters of the Prototype LIM.

Parameter	Symbol	Value
Nominal power	P_n	3 kW
Rated voltage	$V_{L\text{-}L}$	180 V
Nominal linear velocity (mechanical)	v_m	2 m/sec
Rated thrust	F_e	250 N
Rated current	I	14.2 A
Secondary windings resistance	R_r	3.5315 Ω
Mass of the mover	M	2.78 kg
Pole pitch	τ_p	27 mm

from Figs. 17 (a) and (b). The value of the primary flux linkage based on the MTPA and the LMC is illustrated in Fig. 17 (c). The optimum value of the primary flux linkage is different from each other, hence the angle difference between the primary current and the secondary flux linkage is different as shown in Fig. 17 (d). Therefore, the consumed primary current based on the MTPA is lower than the supplied by the LMC as observed from Figs. 17 (e) and (f). This confirms that the MTPA is better than the LMC.

B. EXPERIMENTAL RESULTS

In this subsection, the experimental validation of the SMC and the PI control in the outer control loop are presented for two cases, variable speed at no load, and variable speed at constant load. The main parameters of the 3 kW LIM are listed in Table 4.

The first case is presented in Figs. 18 and 19 for PI and SMC, respectively. Figs. 18 (a) and 19 (a) illustrate the reference speed, actual speed, and the speed tracking error. For speed control loop based on PI, it can be noticed that the speed tracking error varies and has an overshot during speed change, but for the SMC it is approximately fixed. The responses of the reference thrust, and actual thrust are illustrated in Figs. 18 (b) and 19 (b), separately. The secondary position angles for the two control methods are also presented in Figs. 18 (c) and 19 (c), separately. Meanwhile, the second case is used to verify the proposed control system under both

TABLE 5. Comparison between the two control methods in terms of speed tracking error.

Control method	PI	SMC
No load	0.01 m/s	0.001 m/s
Load	0.04 m/s	0.03 m/s

variable linear speed and variable thrust load. Besides, output responses from the proposed SMC are compared with output response from the PI controller as illustrated in Figs. 20 and 21, separately. In this case, the reference speed increases in ramp waveform from standstill up to 2 m/s and it is kept at 2 m/s for 1.5 s then it is decrease again to zero. During this speed variation, the load is also varying where the motor starts with no load for 0.75 s then it is loaded with 300 N for 1 s then it is unloaded for the next 0.75 s. Figures. 20(a) and 21(a) show the reference and the actual together and the speed tracking error between both. It can be noticed from the speed tracking error; the SMC has lower disturbance and smaller overshoot with perfect and faster tracking. Meanwhile, the reference thrust load and the developed thrust from the motor are shown in Figs. 20 (b) and 21(b) for both SMC and PI control respectively. The developed thrust based on the SMC achieves the required thrust load without much distortion and good tracking. Finally, the secondary position angles for both control methods are illustrated in Figs. 20(c) and 21(c), separately. The position of the secondary angle is much clearer when using SMC compared to PI control. The same conclusion can be obtained, where the SMC is better than the PI control when it is used for the outer control loop. For a faster conclusion, Table 5 illustrates the comparison values between the two control methods in terms of the speed tracking error.

Furthermore, the third case study is used to check the capability of the MTPA. In this case the speed is set to 1.5 m/s while the thrust load is 175 N as illustrated from Figs. 22 (a) and (b). After applying the MTPA, the primary current is decreased as the reference value of the primary flux linkage is changed as illustrated from Figs. 22 (c) and (d).

VII. CONCLUSION

This paper has proposed one improved SMC combined with finite-control-set model predictive flux control (FCS-MPFC). Moreover, the optimum value of the primary flux linkage for both maximum thrust per ampere (MTPA) and field weakening (FW) has proposed to improve the drive performance of the LIM drive system in a wide speed range over the rated value. Aided with the FOC, the optimum value of the primary flux linkage is obtained for both MTPA and FW. The proposed FCS-MPFC is based only on the primary flux linkage in the cost function, hence the weighting factor can be removed. Extensive simulation and experimental results are presented for the two control methods (PI and SMC) with and without MTPA based FCS-MPFC. Comprehensive simulation and experimental results have validated the proposed control methods to successfully remove the required time in selecting the weighting factor and achieve a quicker dynamic response. Moreover, the SMC is applied in the outer speed control loop to achieve excellent speed response, where the actual speed reaches the reference value by 10% quicker than the PI controller and with a lower steady-state error of 0.006%. compared to a 0.25% steady-state error in the PI. Thankfully, the MPC would discover more and more prospects for industrial applications at the same time due to the rapid technological evolution of microcontrollers, digital signal processors, and other devices. In addition, MPC can be extended to be used in different applications such as energy management and regenerative braking in EVs/HEVs, the combining with an advanced optimization control, the use in renewable energy like PV and wind. Meanwhile, this work has a future work of applying the MPC with the recent doubly fed linear induction machine and combining it with the recent reaching law of the sliding mode control.

REFERENCES

[1] I. Boldea, L. N. Tutelea, W. Xu, and M. Pucci, "Linear electric machines, drives and MAGLEVs: An overview," *IEEE Trans. Ind. Electron.*, vol. 65, no. 9, pp. 7504–7515, Sep. 2018.

[2] M. F. Elmorshedy, W. Xu, S. M. Allam, J. Rodriguez, and C. Garcia, "MTPA-based finite-set model predictive control without weighting factors for linear induction machine," *IEEE Trans. Ind. Electron.*, vol. 68, no. 3, pp. 2034–2047, Mar. 2021.

[3] W. Xu, M. F. Elmorshedy, Y. Liu, M. R. Islam, and S. M. Allam, "Finite-set model predictive control based thrust maximization of linear induction motors used in linear metros," *IEEE Trans. Veh. Technol.*, vol. 68, no. 6, pp. 5443–5458, Jun. 2019.

[4] W. Xu, J. Zhu, Y. Guo, L. Tan, and S. Wang, "Analysis on performance of linear induction motor basing on winding function method," in *Proc. 4th IEEE Conf. Ind. Electron. Appl.*, Xi'an, China, May 2009, pp. 3639–3642.

[5] M. F. Elmorshedy, W. Xu, Y. Liu, S. M. Allam, M. M. Ali, and M. Dong, "Sensorless direct thrust control of a linear induction motor based on MRAS," in *Proc. 12th Int. Symp. Linear Drives Ind. Appl. (LDIA)*, Neuchatel, Switzerland, Jul. 2019, pp. 1–6.

[6] W. Xu, J. G. Zhu, Y. Zhang, Y. Li, Y. Wang, and Y. Guo, "An improved equivalent circuit model of a single-sided linear induction motor," *J. IEEE Trans. Veh. Technol.*, vol. 59, no. 5, pp. 2277–2289, Jun. 2010.

[7] I. Boldea, *Linear Electric Machines Drives and Maglevs Handbook*. Boca Raton, FL, USA: CRC Press, 2013.

[8] H. Karimi, S. Vaez-Zadeh, and F. R. Salmasi, "Combined vector and direct thrust control of linear induction motors with end effect compensation," *IEEE Trans. Energy Convers.*, vol. 31, no. 1, pp. 196–205, Mar. 2016.

[9] F. Alonge, M. Cirrincione, M. Pucci, and A. Sferlazza, "Input-output feedback linearization control with on-line MRAS-based inductor resistance estimation of linear induction motors including the dynamic end effects," *IEEE Trans. Ind. Appl.*, vol. 52, no. 1, pp. 254–266, Jan. 2016.

[10] G. Lv, D. Zeng, T. Zhou, and Z. Liu, "Investigation of forces and secondary losses in linear induction motor with the solid and laminated back iron secondary for metro," *IEEE Trans. Ind. Electron.*, vol. 64, no. 6, pp. 4382–4390, Jun. 2017.

[11] Q. Lu, Y. Li, Y. Ye, and Z. Q. Zhu, "Investigation of forces in linear induction motor under different slip frequency for low-speed maglev application," *IEEE Trans. Energy Convers.*, vol. 28, no. 1, pp. 145–153, Mar. 2013.

[12] W. Xu, G. Sun, G. Wen, Z. Wu, and P. K. Chu, "Equivalent circuit derivation and performance analysis of a single-sided linear induction motor based on the winding function theory," *IEEE Trans. Veh. Technol.*, vol. 61, no. 4, pp. 1515–1525, May 2012.

[13] Y. Jiang, W. Xu, and C. Ye, "Composite field-oriented control for linear induction motor based super-twisting sliding mode observers," in *Proc. IEEE Conf. Electromagn. Field Comput. (CEFC)*, Miami, FL, USA, Nov. 2016, p. 1.

[14] M. F. Elmorshedy, W. Xu, and Y. Liu, "Speed control of linear induction motor with thrust and stator flux ripple reduction," in *Proc. 21st Int. Conf. Electr. Mach. Syst. (ICEMS)*, Seoul, South Korea, Oct. 2018, pp. 1789–1794.

[15] T. Mir, B. Singh, and A. H. Bhat, "FS-MPC-based speed sensorless control of matrix converter fed induction motor drive with zero common mode voltage," *IEEE Trans. Ind. Electron.*, vol. 68, no. 10, pp. 9185–9195, Oct. 2021.

[16] J. Su, R. Gao, and I. Husain, "Model predictive control based field-weakening strategy for traction EV used induction motor," *IEEE Trans. Ind. Appl.*, vol. 54, no. 3, pp. 2295–2305, May 2018.

[17] M. Mousavi, A. Davari, V. Nekoukar, C. Garcia, and J. Rodriguez, "A robust torque and flux prediction model by a modified disturbance rejection method for finite-set model-predictive control of induction motor," *IEEE Trans. Power Electron.*, vol. 36, no. 8, pp. 9322–9333, Aug. 2021.

[18] A. A. Ahmed, B. K. Koh, and Y. Il Lee, "A comparison of finite control set and continuous control set model predictive control schemes for speed control of induction motors," *IEEE Trans. Ind. Informat.*, vol. 14, no. 4, pp. 1334–1346, Apr. 2018.

[19] M. F. Elmorshedy, W. Xu, F. F. El-Sousy, M. R. Islam, and A. A. Ahmed, "Recent achievements in model predictive control techniques for industrial motor: A comprehensive state-of-the-art," *IEEE Access*, vol. 9, pp. 58170–58191, 2021.

[20] W. Xu, M. F. Elmorshedy, Y. Liu, J. Rodriguez, and C. Garcia, "Maximum thrust per ampere of linear induction machine based on finite-set model predictive direct thrust control," *IEEE Trans. Power Electron.*, vol. 35, no. 7, pp. 7366–7378, Jul. 2020.

[21] F. Wang, S. Li, X. Mei, W. Xie, and J. Rodríguez, "Model-based predictive direct control strategies for electrical drives: An experimental evaluation of PTC and PCC methods," *IEEE Trans. Ind. Informat.*, vol. 11, no. 3, pp. 671–681, Jun. 2015.

[22] W. Xie, X. Wang, F. Wang, W. Xu, R. M. Kennel, and D. Gerling, "Finite-control-set model predictive torque control with a deadbeat solution for PMSM drives," *IEEE Trans. Ind. Electron.*, vol. 62, no. 9, pp. 5402–5410, Sep. 2015.

[23] Y. Zhang, J. Jin, and L. Huang, "Model-free predictive current control of PMSM drives based on extended state observer using ultralocal model," *IEEE Trans. Ind. Electron.*, vol. 68, no. 2, pp. 993–1003, Feb. 2021, doi: 10.1109/TIE.2020.2970660.

[24] M. Norambuena, J. Rodriguez, Z. Zhang, F. Wang, C. Garcia, and R. Kennel, "A very simple strategy for high-quality performance of AC machines using model predictive control," *IEEE Trans. Power Electron.*, vol. 34, no. 1, pp. 794–800, Jan. 2019.

[25] M. F. Elmorshedy, M. Rabiul Islam, W. Xu, F. F. M. El-Sousy, and S. Arslan Bukhari, "Fast linear speed response based on SMC with finite-control-set model predictive flux control for linear induction motor," in *Proc. IEEE Ind. Appl. Soc. Annu. Meeting (IAS)*, Oct. 2021, pp. 1–6.

[26] M. Preindl and S. Bolognani, "Model predictive direct torque control with finite control set for PMSM drive systems, Part 1: Maximum torque per ampere operation," *IEEE Trans. Ind. Informat.*, vol. 9, no. 4, pp. 1912–1921, Nov. 2013.

[27] M. Habibullah, D. D.-C. Lu, D. Xiao, and M. F. Rahman, "A simplified finite-state predictive direct torque control for induction motor drive," *IEEE Trans. Ind. Electron.*, vol. 63, no. 6, pp. 3964–3975, Jun. 2016.
[28] R. Vargas, U. Ammann, B. Hudoffsky, J. Rodríguez, and P. Wheeler, "Predictive torque control of an induction machine fed by a matrix converter with reactive input power control," *IEEE Trans. Power Electron.*, vol. 25, no. 6, pp. 1426–1438, Jun. 2010.
[29] S. A. Davari, "Predictive direct angle control of induction motor," *IEEE Trans. Ind. Electron.*, vol. 63, no. 8, pp. 5276–5284, Aug. 2016, doi: 10.1109/TIE.2016.2551198.
[30] W. Xu, J. Zou, Y. Liu, and J. Zhu, "Weighting factorless model predictive thrust control for linear induction machine," *IEEE Trans. Power Electron.*, vol. 34, no. 10, pp. 9916–9928, Oct. 2019.
[31] F. Wang, H. Xie, Q. Chen, S. A. Davari, J. Rodriguez, and R. Kennel, "Parallel predictive torque control for induction machines without weighting factors," *IEEE Trans. Power Electron.*, vol. 35, no. 2, pp. 1779–1788, Feb. 2020.

MAHMOUD F. ELMORSHEDY (Member, IEEE) was born in Gharbeya, Egypt, in 1989. He received the B.Sc. and M.Sc. degrees in electrical engineering from Tanta University, Egypt, in 2012 and 2016, respectively, and the Ph.D. degree in electrical engineering from the School of Electrical and Electronic Engineering, Huazhong University of Science and Technology, China, in 2020. He was a Teaching Assistant with the Department of Electrical Power and Machines Engineering, Faculty of Engineering, Tanta University, in 2013, where he was promoted to Assistant Lecturer, in June 2016. He is currently an Assistant Professor (on academic leave) with the Department of Electrical Power and Machines Engineering, Faculty of Engineering, Tanta University. He is also a Postdoctoral Fellow with the Renewable Energy Laboratory, College of Engineering, Prince Sultan University, Riyadh, Saudi Arabia. His research interests include linear induction motors, predictive control, power electronics, and renewable energy.

DHAFER J. ALMAKHLES (Senior Member, IEEE) received the B.E. degree in electrical engineering from the King Fahd University of Petroleum and Minerals, Dhahran, Saudi Arabia, in 2006, and the master's (Hons.) and Ph.D. degrees from The University of Auckland, New Zealand, in 2011 and 2016, respectively. Since 2016, he has been with Prince Sultan University, Saudi Arabia, where he is currently the Chairperson of the Communications and Networks Engineering Department and the Director of the Science and Technology Unit. He is also a Leader of the Renewable Energy Research Team and the Renewable Energy Laboratory, Prince Sultan University. His research interests include the hardware implementation of control theory, signal processing, networked control systems, and sliding mode.

FAYEZ F. M. EL-SOUSY (Member, IEEE) received the B.Sc. degree in electrical engineering from Menoufia University, Egypt, in 1988, and the M.Sc. and Ph.D. degrees in electrical engineering from Cairo University, Giza, Egypt, in 1994 and 2000, respectively. From August 1995 to June 2000, he was a Lecturer with the Department of Electrical Engineering, October Six University, Giza. From August 2000 to June 2003, he was an Assistant Professor with the Department of Electrical Engineering, October Six University. From April 2004 to February 2007, he was a Postdoctoral Visiting Researcher with the Graduate School of Information Science and Electrical Engineering, Kyushu University, Fukuoka, Japan. From 2007 to 2010, he was an Associate Professor and the Chair of the Electrical Engineering Department, College of Engineering, King Saud University, Riyadh, Saudi Arabia. From 2010 to 2014, he was an Associate Professor and the Chair of the Electrical Engineering Department, College of Engineering, Prince Sattam bin Abdulaziz University, Al-Kharj, Saudi Arabia. Since 2014, he has been a Full Professor and the Chair of the Electrical Engineering Department, College of Engineering, Prince Sattam bin Abdulaziz University. His research interests include the modeling and control of motor drives, motion-control systems, wind energy systems, digital signal processing-based computer control systems, computational intelligence of power electronics, electric drives and power systems, intelligent control theories including fuzzy logic, neural networks, and wavelets, nonlinear control, optimal control, and robust control.